NANO LETTERS
Cite This: Nano Lett. 2019, 19, 1009−1014
Letter
pubs.acs.org/NanoLett

Hyperbolic Phonon Polaritons in Suspended Hexagonal Boron Nitride

Siyuan Dai,[†] Jiamin Quan,[‡] Guangwei Hu,[§,∥] Cheng-Wei Qiu,[§] Tiger H Tao,[⊥] Xiaoqin Li,[‡] and Andrea Alù*[,†,∥,#,▽]

[†]Department of Electrical & Computer Engineering, The University of Texas at Austin, Austin, Texas 78712, United States
[‡]Department of Physics, The University of Texas at Austin, Austin, Texas 78712, United States
[§]Department of Electrical and Computer Engineering, National University of Singapore, Kent Ridge, Singapore 117583, Republic of Singapore
[∥]Photonics Initiative, Advanced Science Research Center, City University of New York, New York 10031, United States
[⊥]Department of Mechanical Engineering, The University of Texas at Austin, Austin, Texas 78712, United States
[#]Physics Program, Graduate Center, City University of New York, New York 10016, United States
[▽]Department of Electrical Engineering, City College of The City University of New York, New York 10031, United States

ABSTRACT: Highly confined and low-loss hyperbolic phonon polaritons in hexagonal boron nitride possess properties analogous to surface plasmon polaritons, but with enhanced confinement and lower loss. Their properties have been so far mostly studied on dielectric substrates, which provide an asymmetric environment for polariton propagation, and add to damping. In this work, we investigate hyperbolic phonon polaritons over suspended hexagonal boron nitride, showing remarkable properties, including elongated polariton wavelength and reduced damping, up to 18% lower compared to dielectric-backed samples. We use real-space nanoimaging of the polaritons in hexagonal boron nitride to demonstrate and visualize these effects. Our results indicate that suspended boron nitride offers better figures of merit for polariton transport, which are generalizable to other polaritonic materials, and they may be explored in heterostructures for advanced nanophotonic applications.

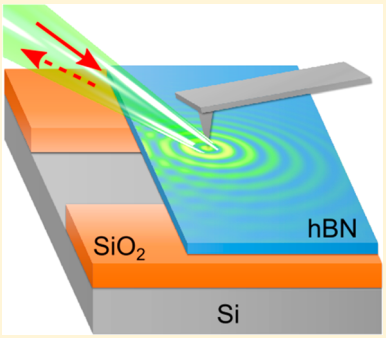

KEYWORDS: *Polaritons, propagation elongation, suspended van der Waals crystals, hexagonal boron nitride*

Hexagonal boron nitride (hBN) is a representative van der Waals (vdW) crystal,[1] in which atomic layers are bonded together by weak vdW forces. Thanks to its high chemical stability,[2] insulating nature, and clean and atomically flat surface,[3] hBN has been widely used in nanoelectronics as an excellent substrate and dielectric spacer.[4] For electronic applications, heterostructures combining hBN and other vdW crystals have been shown to support ultrahigh electron mobility[3,5] and can protect sensitive materials in atmosphere.[6,7] In addition to electronics, hBN also offers interesting properties for photonics and plasmonics. It emits ultraviolet light[8,9] and can host a variety of defects functioning as single photon emitters.[10] In the mid-infrared spectrum, hBN is a natural hyperbolic material, and it supports hyperbolic phonon polaritons.[11−18] While phonon polaritons and plasmon polaritons are both hybrid light-matter propagating modes,[19,20] the former provide larger optical confinement and lower damping. Hyperbolic phonon polaritons in hBN have therefore led to a series of advances in nanophotonics, including subdiffractional focusing,[21,22] biochemical sensing,[23] flat optics,[17,18] internal structure analysis,[24] and a natural platform for metamaterials and metasurfaces.[25] In order to achieve a tunable hyperbolic response and to expand the functionality of hBN polaritonic devices, the modification of hBN polaritons combining hBN with other materials has also been investigated.[4] Representative previous results have reported the tuning of polaritons in hBN with a plasmonic graphene layer[26] and with phase change materials.[27] However, these effects are often accompanied by deteriorative damping in hyperbolic phonon polaritons due to added material loss intrinsic in the surrounding materials. A recent work has demonstrated loss compensation[28] of hyperbolic phonon polaritons in hBN via isotropic enrichment, in order to reduce the phonon-defect scattering for propagating polariton waves.

While it appears promising to explore low-loss and flat substrates, such as silicon nitride[29] in order to improve the figures of merits for propagating polaritons, in this work we investigate the modification of hyperbolic phonon polaritons by suspending hBN crystals. The modification is directly observed with infrared nanoimaging and confirmed in theory and simulations. This modification of polariton properties can be attributed to a change of dielectric environment for the supported hyperbolic phonon polaritons. While we achieve

Received: October 21, 2018
Revised: December 13, 2018
Published: December 14, 2018

DOI: 10.1021/acs.nanolett.8b04242
Nano Lett. 2019, 19, 1009−1014

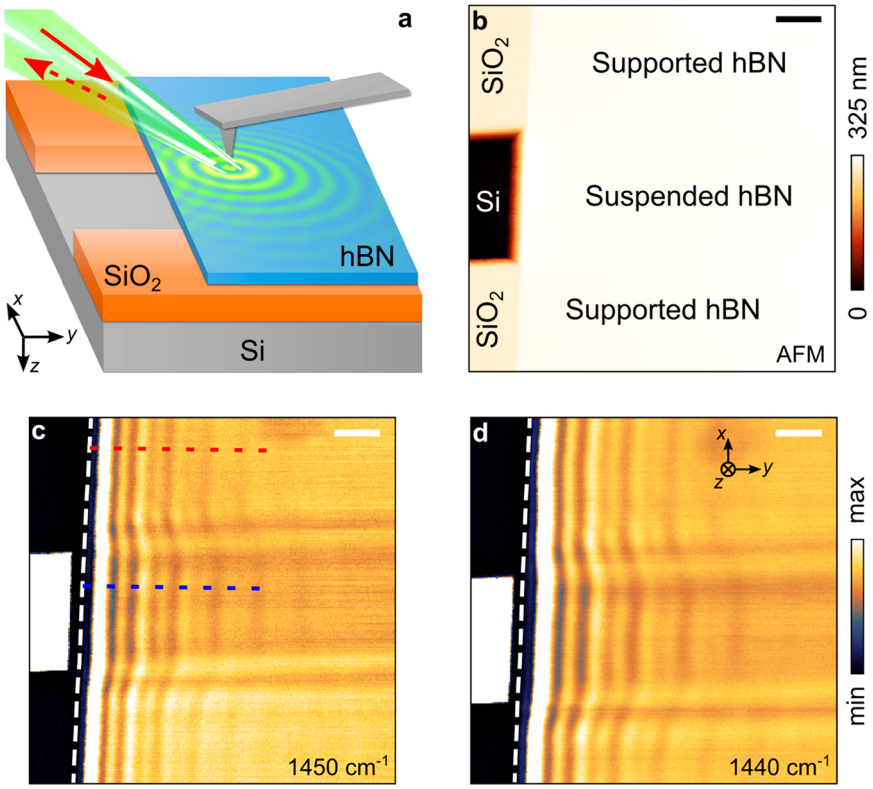

Figure 1. Schematic and s-SNOM images of hyperbolic phonon polaritons in hexagonal boron nitride. (a) Experiment setup. An exfoliated microcrystal of hBN was transferred onto the Si/SiO_2 substrate with an air trench such that part of the hBN was suspended. In the experiment, the AFM tip is illuminated (red solid arrow) by an infrared (IR) beam from QCL. We collect the backscattered IR signal (red dashed arrow). (b) AFM image of the suspended and supported hBN studied in our experiment. (c), (d) s-SNOM images of the suspended and supported hBN slab at ω = 1450 cm^{-1} (c) and 1440 cm^{-1} (d). Red and blue dashed lines track line cuts of the s-SNOM data; the corresponding profiles are presented in Figure 2a. Scale bar: 500 nm.

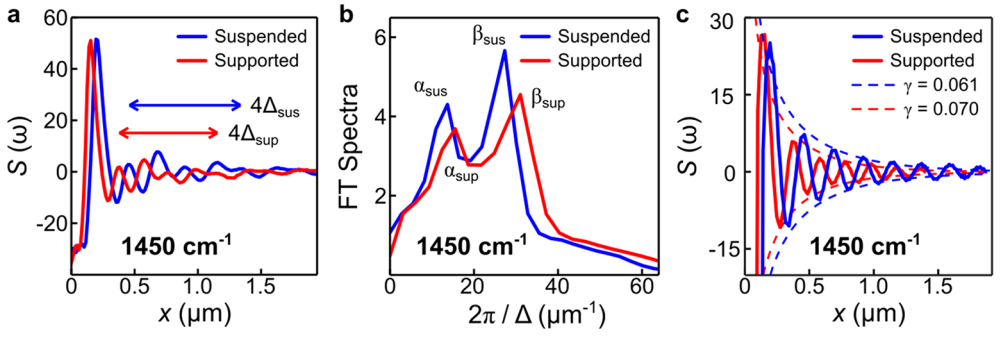

Figure 2. s-SNOM line profiles for hyperbolic phonon polaritons in suspended (blue) and supported (red) hBN. (a) s-SNOM line profiles taken along the dashed cuts in Figure 1c, the fringe periods are indicated with double arrows (blue and red arrow for Δ_{sus} and Δ_{sup}, respectively). (b) Fourier transform spectra of the s-SNOM line profile in Figure 2a. α and β indicate peaks in the FT spectra. (c) $\Delta = \lambda_p/2$ line profiles and the corresponding damping factor γ. The line profiles were obtained by inverse Fourier transform of the spectra in Figure 2b. IR frequency ω = 1450 cm^{-1}.

tuning of the polariton wavelength, we are also able to reduce the polariton damping because of the elimination of substrate loss in the suspended geometry. Thus, this technique opens interesting opportunities to improve the performance of polaritonic nanodevices.

The schematic of our infrared nanoimaging experiments on suspended hBN is shown in Figure 1a. Our substrate comprises two layers: a doped Si wafer (gray) capped with a 285 nm thick SiO_2 (orange). The capped SiO_2 layer was patterned to contain 1.5 μm wide air trenches by reactive ion etching. hBN crystals were then mechanically exfoliated from bulk samples and transferred to the substrate, such that part of the hBN crystal remained suspended (Figure 1a). The infrared nanoimaging experiment was performed using a scattering-type scanning near-field optical microscope (s-SNOM, www.neaspec.com) and quantum cascade lasers (QCLs, www.daylightsolutions.com). In the s-SNOM nanoimaging, the PtIr coated atomic force microscope (AFM) tip (radius ~20 nm) was set to tapping mode with a frequency ~270 kHz and amplitude ~70 nm. When the sample was scanned underneath, we illuminated the AFM tip with the QCL and collected the backscattered optical signal. The scattered signal was then collected in a

DOI: 10.1021/acs.nanolett.8b04242
Nano Lett. 2019, 19, 1009−1014

pseudoheterodyne interferometric detection module,[30] such that the AFM topography (Figure 1b), s-SNOM amplitude ($s(\omega)$, Figure 1c,d), and s-SNOM phase could be recorded simultaneously. In order to obtain the genuine near-field signal, we then demodulated the s-SNOM output at the third harmonics of the tip tapping frequency.

In the experiment, once illuminated with the QCL, the AFM tip acts as an optical antenna that conveys the energy of the incident photons and launches hyperbolic phonon polaritons (Figure 1a) with a wavelength λ_p much smaller than the one of free-space photons λ_0. Here $\lambda_0 = 1/\omega$, where ω is the QCL emission frequency in wavenumbers (cm^{-1}). Hyperbolic phonon polaritons are propagating waves in hBN, and they can be recognized in the observed s-SNOM images (Figure 1c,d) as periodic oscillations (fringes). Similar to previous works,[28,31] the polariton fringes usually exhibit a period $\Delta = \lambda_p/2$ close to the hBN edge (white dashed line). The s-SNOM line profiles, taken along dashed lines in the s-SNOM image (Figure 1c), are plotted in Figure 2a. The polariton fringes appear as oscillation peaks and show the strongest oscillations next to the edge ($x = 0$), followed by a series of weakly damped ones. These fringes originate from the standing wave interference between tip-launched polaritons and edge-reflected polaritons. The $\Delta = \lambda_p/2$ fringes are actually superpositioned with weak $\Delta = \lambda_p$ fringes in the images, as confirmed by the appearance of α ($\Delta = \lambda_p$) and β ($\Delta = \lambda_p/2$) peaks in the corresponding Fourier transform (FT) spectra in Figure 2b. As studied in previous works, the $\Delta = \lambda_p$ fringes are attributed to polaritons launched by the crystal edge.[31,32] Because the $\Delta = \lambda_p/2$ fringes dominate in the s-SNOM images, the following analysis will rely mainly on the $\lambda_p/2$ fringes.

On the basis of this experimental technique, we now analyze the properties of hyperbolic phonon polaritons observed in suspended and supported hBN. Polariton fringes are observed in both suspended and supported hBN (Figure 1c,d). They appear to support similar oscillations, as displayed in the s-SNOM line profiles (Figure 2a). Interestingly, although the suspended and supported hBN are in the same crystal and show no topographic difference (Figure 1b), the polariton wavelength in the suspended hBN is longer than the one in the supported hBN: $\lambda_{sus} > \lambda_{sup}$. This wavelength difference is unambiguously revealed in the s-SNOM line profiles and the corresponding FT spectra, as seen in the difference between Δ_{sus} (blue arrow, Figure 2a) and Δ_{sup} (red arrows) and the difference between β_{sus} and β_{sup} (Figure 2b). A direct implication of the fact that $\lambda_{sus} > \lambda_{sup}$, observable in the s-SNOM images (Figure 1c,d), is that polariton fringes in the suspended part are bent toward the crystal interior compared with those in the supported part.

We attribute the difference between λ_{sus} and λ_{sup} to the change of permittivity in the polariton substrate: from SiO_2 $\varepsilon_{SiO_2} = 1.22 + 0.02i$ to air $\varepsilon_{air} = 1$ at this frequency $\omega = 1450$ cm^{-1}. The dispersion of hyperbolic phonon polaritons in hBN can be derived using the Fabry–Perot quantization condition, which yields[11]

$$k = k_1 + ik_2 = -\frac{\psi}{d}\left[\arctan\left(\frac{1}{\varepsilon_x\psi}\right) + \arctan\left(\frac{\varepsilon_s}{\varepsilon_x\psi}\right) + \pi l\right]$$

$$\psi = \frac{\sqrt{\varepsilon_z}}{i\sqrt{\varepsilon_x}} \quad (1)$$

where d is the hBN thickness, $l = 0, 1, 2, 3, \ldots$ is the branch index of hyperbolic phonon polaritons. ε_s is the permittivity of the substrate, and $\varepsilon_x = \varepsilon_y = \varepsilon_t$ and ε_z are principal components of the hBN permittivity tensor. $k = k_1 + ik_2$ is the complex in-plane momentum of polaritons and relates to the polariton wavelength by $k_1 = 2\pi/\lambda_p$. As described by eq 1, the polariton wavelength λ_p depends on the substrate permittivity ε_s. Specifically, in the upper Reststrahlen band $\mathrm{Im}\,\varepsilon_z \sim 0$, one obtains

$$\frac{\partial k_1}{\partial \varepsilon_s} = \frac{1}{d}\frac{\varepsilon_z[\mathrm{Re}(\varepsilon_s^2) - \varepsilon_z\,\mathrm{Re}(\varepsilon_t)]}{|\varepsilon_s^2 - \varepsilon_z\varepsilon_t|^2} \quad (2)$$

For $\varepsilon_{SiO_2} = 1.22 + 0.02i$ and air $\varepsilon_{air} = 1$, $\frac{\partial k_1}{\partial \varepsilon_s} > 0$; therefore, $\lambda_{sus} > \lambda_{sup}$. In our experiment, the modification of polariton wavelength by sample suspending can also be observed at other frequencies (e.g., $\omega = 1440$ cm^{-1} in Figure 1d) and spans over the whole upper Reststrahlen band of hBN. We outline the dispersion of λ_{sus} and λ_{sup} from the same crystal by plotting the frequency (ω) − wavelength (λ_p/λ_0) dispersion in Figure 3b. The simulation results (blue and red curves, using ε_{air} and ε_{SiO_2}) excellently match our experimental data (blue dots and red squares).

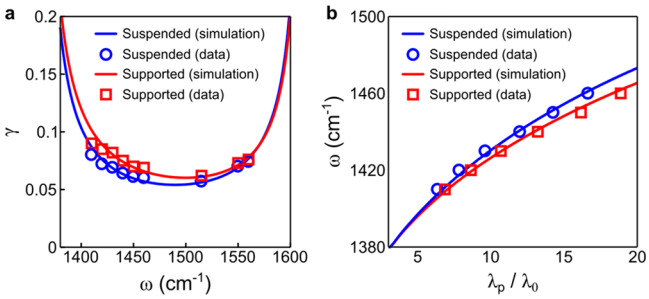

Figure 3. Polariton damping and wavelength. (a) Dependence of polariton damping γ as a function of frequency ω. (b) Dependence of polariton wavelength λ_p as a function of frequency ω. Experimental data are indicated with blue dots (suspended hBN) and red squares (supported hBN) whereas the simulation results are plotted with blue (suspended hBN) and red (supported hBN) curves.

We now demonstrate that not only the polariton wavelength λ_p is modified by the sample suspension but also the polariton damping γ is reduced in this geometry. A reasonable figure of merit for the polariton damping, $\gamma = k_2/k_1$, describes the decay of oscillation amplitude of propagating polariton waves normalized to the wavelength. In the experiment, the polariton damping γ can be obtained by fitting the s-SNOM line profile with the sinusoidal wave function $s(\omega) = Ax^{-1/2}e^{2kx}$.[31,32] To remove the influence of $\Delta = \lambda_p$ fringes, we performed the inverse FT of the β peak (Figure 2b), such that the output data (Figure 2c) contain the genuine $\Delta = \lambda_p/2$ fringes. At a representative frequency $\omega = 1450$ cm^{-1}, we extracted $\gamma_{sus} = 0.061$ whereas $\gamma_{sup} = 0.070$, as shown by the fitting envelop es in Figure 2c. Following the same procedure, we observe a reduction of polariton damping over a broad range in the Reststrahlen band (Figure 3a), with excellent agreement between simulation results (blue and red curve) from eq 1 and experimental data (blue dots and red squares). This polariton loss reduction $\gamma_{sus} < \gamma_{sup}$ is attributed to the removal of dielectric loss of the substrate in the suspended geometry.

DOI: 10.1021/acs.nanolett.8b04242
Nano Lett. 2019, 19, 1009−1014

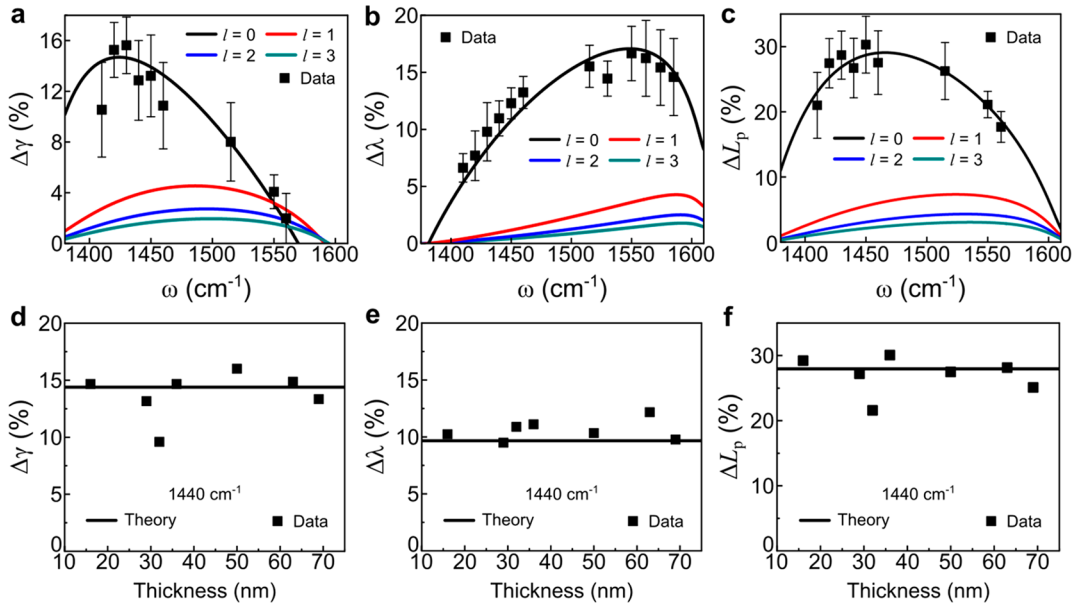

Figure 4. Coefficient of polariton damping reduction, wavelength and propagation length elongation by sample suspension. (a) Coefficient of polariton damping reduction $\Delta\gamma(\%)$ as a function of frequency ω. (b) Coefficient of polariton wavelength elongation $\Delta\lambda(\%)$ as a function of frequency ω. (c) Coefficient of polariton propagation length elongation $\Delta L_p(\%)$ as a function of frequency ω. (d) Thickness dependence of $\Delta\gamma(\%)$ at a representative frequency ω = 1440 cm^{-1}. (e) Thickness dependence of $\Delta\lambda(\%)$ at a representative frequency ω = 1440 cm^{-1}. (f) Thickness dependence of $\Delta\lambda(\%)$ at a representative frequency ω = 1440 cm^{-1}. Simulations are shown as color curves while the experimental results are plotted with black squares. l = 0, 1, 2, and 3 indicate different branches of hyperbolic phonon polaritons in hBN. The error bars in Figure 4a–c originate from uncertainty in the measurement of polariton wavelength (Figure 2a) and fitting of the polariton line trace (Figure 2c) with our simulation.

Having demonstrated the modification of wavelength and damping of hyperbolic phonon polaritons by sample suspension, we quantify these modifications by defining the coefficient for wavelength elongation $\Delta\lambda = |\lambda_{sup} - \lambda_{sus}|/\lambda_{sup}$ and damping reduction $\Delta\gamma = |\gamma_{sup} - \gamma_{sus}|/\gamma_{sup}$. On the basis of wavelength λ and damping γ, we further extract the polariton propagation length $L_p = (2k_2)^{-1} = \lambda/4\pi\gamma$ and the propagation length elongation coefficient $\Delta L_p = |L_{p\,sup} - L_{p\,sus}|/L_{p\,sup}$. In Figure 4, we plot both the experimental data (black squares) extracted from Figures 1–3 and simulations from eq 1 for $\Delta\lambda$, $\Delta\gamma$, and ΔL_p. We provide three important results. First is the modification coefficient $\Delta\lambda$, where $\Delta\gamma$ ranges from 0 to 20% and ΔL_p ranges from 0 to 30% and they all vary with frequency in the Reststrahlen band. Second is the damping reduction, where wavelength and propagation length elongation via sample suspension are most effective for the l = 0 branch of the hyperbolic phonon polaritons: as the branch index l (see l = 1, 2, and 3 curves in Figure 4a,b) increases, the polariton modification effects ($\Delta\lambda$, $\Delta\gamma$, and ΔL_p) decreases. The different modification effects for different polariton branches are related to their spatial field distribution:[26,33] as l increases, the electromagnetic field of polaritons is better confined inside the hBN slab; therefore, it is less sensitive to the environmental permittivity change (e.g., sample suspending in this work). Third, once the frequency ω is fixed, the modified coefficients $\Delta\lambda$, $\Delta\gamma$, and ΔL_p stay universal for hBN crystals of different thicknesses, as verified in our experiments and simulations (Figure 4c,d).

In summary, using infrared nanoimaging and detailed electromagnetic simulations, we have investigated hyperbolic phonon polaritons in suspended hBN. We demonstrated that sample suspension can effectively reduce the polariton damping and elongate the wavelength and propagation length of the polaritons by eliminating the substrate loss and changing the environment permittivity. In our experiment, the damping reduction $\Delta\gamma$ reaches 18% in the suspended geometry, thus, providing better figures of merits for hyperbolic phonon polaritons. Sample suspension to modify polariton wavelength and reduce damping, as introduced in this work, is expected to be generalizable to other polaritonic media, such as low-dimensional materials[20,34] including graphene,[35,36] transition metal dichalcogenides,[37,38] topological insulators,[39] black phosphorus,[40] and nanowires[41,42] as well as conventional plasmonic systems including metals and metamaterials.[43] The modification of polaritons by changing the dielectric environment, such as sample suspension, may be further engineered and programmed in order to achieve sophisticated nano-photonic functionalities, including propagation steering and transformation polaritonics.[44]

AUTHOR INFORMATION

Corresponding Author

*A. Alù. E-mail: aalu@gc.cuny.edu.

ORCID

Siyuan Dai: 0000-0001-7259-7182

Andrea Alù: 0000-0002-4297-5274

Notes

The authors declare no competing financial interest.

ACKNOWLEDGMENTS

S.D. and A.A. were supported by the AFOSR MURI grant number FA9550-17-1-0002, the DARPA Nascent program, and the Welch Foundation with grant No. F-1802. X. Li gratefully acknowledges Welch grant F-1662 and NSF DMR-1808042. The collaboration between X.L. and A.A is facilitated

DOI: 10.1021/acs.nanolett.8b04242
Nano Lett. 2019, 19, 1009–1014

by the NSF MRSEC program DMR-1720595. J.Q. acknowledges the support from the China Scholarship Council (Grant No. 201706050068). C.-W.Q. acknowledges the financial support from A*STAR Pharos Program (grant no. 152 70 00014, with project no. R-263-000-B91-305).

■ ABBREVIATIONS

s-SNOM, scattering-type scanning near-field optical microscopy; hBN, hexagonal boron nitride; vdW, van der Waals

■ REFERENCES

(1) Novoselov, K. S.; Jiang, D.; Schedin, F.; Booth, T. J.; Khotkevich, V. V.; Morozov, S. V.; Geim, A. K. *Proc. Natl. Acad. Sci. U. S. A.* **2005**, *102* (30), 10451−10453.
(2) Liu, Z.; Gong, Y.; Zhou, W.; Ma, L.; Yu, J.; Idrobo, J. C.; Jung, J.; MacDonald, A. H.; Vajtai, R.; Lou, J.; Ajayan, P. M. *Nat. Commun.* **2013**, *4*, 2541.
(3) Dean, C. R.; Young, A. F.; Meric, I.; Lee, C.; Wang, L.; Sorgenfrei, S.; Watanabe, K.; Taniguchi, T.; Kim, P.; Shepard, K. L.; Hone, J. *Nat. Nanotechnol.* **2010**, *5*, 722.
(4) Geim, A. K.; Grigorieva, I. V. *Nature* **2013**, *499* (7459), 419−425.
(5) Wang, L.; Meric, I.; Huang, P. Y.; Gao, Q.; Gao, Y.; Tran, H.; Taniguchi, T.; Watanabe, K.; Campos, L. M.; Muller, D. A.; Guo, J.; Kim, P.; Hone, J.; Shepard, K. L.; Dean, C. R. *Science* **2013**, *342* (6158), 614−617.
(6) Chen, X.; Wu, Y.; Wu, Z.; Han, Y.; Xu, S.; Wang, L.; Ye, W.; Han, T.; He, Y.; Cai, Y.; Wang, N. *Nat. Commun.* **2015**, *6*, 7315.
(7) Doganov, R. A.; O'Farrell, E. C. T.; Koenig, S. P.; Yeo, Y.; Ziletti, A.; Carvalho, A.; Campbell, D. K.; Coker, D. F.; Watanabe, K.; Taniguchi, T.; Neto, A. H. C.; Özyilmaz, B. *Nat. Commun.* **2015**, *6*, 6647.
(8) Watanabe, K.; Taniguchi, T.; Kanda, H. *Nat. Mater.* **2004**, *3*, 404.
(9) Cassabois, G.; Valvin, P.; Gil, B. *Nat. Photonics* **2016**, *10*, 262.
(10) Tran, T. T.; Bray, K.; Ford, M. J.; Toth, M.; Aharonovich, I. *Nat. Nanotechnol.* **2016**, *11*, 37−41.
(11) Dai, S.; Fei, Z.; Ma, Q.; Rodin, A. S.; Wagner, M.; McLeod, A. S.; Liu, M. K.; Gannett, W.; Regan, W.; Watanabe, K.; Taniguchi, T.; Thiemens, M.; Dominguez, G.; Neto, A. H. C.; Zettl, A.; Keilmann, F.; Jarillo-Herrero, P.; Fogler, M. M.; Basov, D. N. *Science* **2014**, *343* (6175), 1125−1129.
(12) Caldwell, J. D.; Kretinin, A. V.; Chen, Y.; Giannini, V.; Fogler, M. M.; Francescato, Y.; Ellis, C. T.; Tischler, J. G.; Woods, C. R.; Giles, A. J.; Hong, M.; Watanabe, K.; Taniguchi, T.; Maier, S. A.; Novoselov, K. S. *Nat. Commun.* **2014**, *5*, 5221.
(13) Yoxall, E.; Schnell, M.; Nikitin, A. Y.; Txoperena, O.; Woessner, A.; Lundeberg, M. B.; Casanova, F.; Hueso, L. E.; Koppens, F. H. L.; Hillenbrand, R. *Nat. Photonics* **2015**, *9* (10), 674−678.
(14) Shi, Z.; Bechtel, H. A.; Berweger, S.; Sun, Y.; Zeng, B.; Jin, C.; Chang, H.; Martin, M. C.; Raschke, M. B.; Wang, F. *ACS Photonics* **2015**, *2* (7), 790−796.
(15) Dai, S.; Tymchenko, M.; Yang, Y.; Ma, Q.; Pita-Vidal, M.; Watanabe, K.; Taniguchi, T.; Jarillo-Herrero, P.; Fogler, M. M.; Alù, A.; Basov, D. N. *Adv. Mater.* **2018**, *30* (16), 1706358.
(16) Li, P.; Dolado, I.; Alfaro-Mozaz, F. J.; Nikitin, A. Yu.; Casanova, F.; Hueso, L. E.; Vélez, S.; Hillenbrand, R. *Nano Lett.* **2017**, *17* (1), 228−235.
(17) Lin, X.; Yang, Y.; Rivera, N.; López, J. J.; Shen, Y.; Kaminer, I.; Chen, H.; Zhang, B.; Joannopoulos, J. D.; Soljačić, M. *Proc. Natl. Acad. Sci. U. S. A.* **2017**, *114* (26), 6717−6721.
(18) Jiang, Y.; Lin, X.; Low, T.; Zhang, B.; Chen, H. *Laser & Photonics Reviews* **2018**, *12* (5), 1800049.
(19) Giles, A. J.; Dai, S.; Glembocki, O. J.; Kretinin, A. V.; Sun, Z.; Ellis, C. T.; Tischler, J. G.; Taniguchi, T.; Watanabe, K.; Fogler, M. M.; Novoselov, K. S.; Basov, D. N.; Caldwell, J. D. *Nano Lett.* **2016**, *16* (6), 3858−3865.
(20) Low, T.; Chaves, A.; Caldwell, J. D.; Kumar, A.; Fang, N. X.; Avouris, P.; Heinz, T. F.; Guinea, F.; Martin-Moreno, L.; Koppens, F. *Nat. Mater.* **2017**, *16* (2), 182−194.
(21) Dai, S.; Ma, Q.; Andersen, T.; McLeod, A. S.; Fei, Z.; Liu, M. K.; Wagner, M.; Watanabe, K.; Taniguchi, T.; Thiemens, M.; Keilmann, F.; Jarillo-Herrero, P.; Fogler, M. M.; Basov, D. N. *Nat. Commun.* **2015**, *6*, 6963.
(22) Li, P.; Lewin, M.; Kretinin, A. V.; Caldwell, J. D.; Novoselov, K. S.; Taniguchi, T.; Watanabe, K.; Gaussmann, F.; Taubner, T. *Nat. Commun.* **2015**, *6*, 7507.
(23) Autore, M.; Li, P.; Dolado, I.; Alfaro-Mozaz, F. J.; Esteban, R.; Atxabal, A.; Casanova, F.; Hueso, L. E.; Alonso-González, P.; Aizpurua, J.; Nikitin, A. Y.; Vélez, S.; Hillenbrand, R. *Light: Sci. Appl.* **2017**, *7*, 17172.
(24) Dai, S.; Tymchenko, M.; Xu, Z.-Q.; Tran, T. T.; Yang, Y.; Ma, Q.; Watanabe, K.; Taniguchi, T.; Jarillo-Herrero, P.; Aharonovich, I.; Basov, D. N.; Tao, T. H.; Alù, A. *Nano Lett.* **2018**, *18*, 5205.
(25) Li, P.; Dolado, I.; Alfaro-Mozaz, F. J.; Casanova, F.; Hueso, L. E.; Liu, S.; Edgar, J. H.; Nikitin, A. Y.; Vélez, S.; Hillenbrand, R. *Science* **2018**, *359* (6378), 892−896.
(26) Dai, S.; MaQ; Liu, M. K.; AndersenT; FeiZ; Goldflam, M. D.; WagnerM; WatanabeK; TaniguchiT; ThiemensM; KeilmannF; Janssen, G. C. A. M.; Zhu, S. E.; Jarillo Herrero, P.; Fogler, M. M.; Basov, D. N. *Nat. Nanotechnol.* **2015**, *10* (8), 682−686.
(27) Folland, T. G.; Fali, A.; White, S. T.; Matson, J. R.; Liu, S.; Aghamiri, N. A.; Edgar, J. H.; Haglund, R. F.; Abate, Y.; Caldwell, J. D. *ArXiv e-prints* **2018**.
(28) Giles, A. J.; Dai, S.; Vurgaftman, I.; Hoffman, T.; Liu, S.; Lindsay, L.; Ellis, C. T.; Assefa, N.; Chatzakis, I.; Reinecke, T. L.; Tischler, J. G.; Fogler, M. M.; Edgar, J. H.; Basov, D. N.; Caldwell, J. D. *Nat. Mater.* **2017**, *17*, 134.
(29) Stiegler, J. M.; Abate, Y.; Cvitkovic, A.; Romanyuk, Y. E.; Huber, A. J.; Leone, S. R.; Hillenbrand, R. *ACS Nano* **2011**, *5* (8), 6494−6499.
(30) Ocelic, N.; Huber, A.; Hillenbrand, R. *Appl. Phys. Lett.* **2006**, *89* (10), 101124.
(31) Dai, S.; Ma, Q.; Yang, Y.; Rosenfeld, J.; Goldflam, M. D.; McLeod, A.; Sun, Z.; Andersen, T. I.; Fei, Z.; Liu, M.; Shao, Y.; Watanabe, K.; Taniguchi, T.; Thiemens, M.; Keilmann, F.; Jarillo-Herrero, P.; Fogler, M. M.; Basov, D. N. *Nano Lett.* **2017**, *17* (9), 5285−5290.
(32) Woessner, A.; Lundeberg, M. B.; Gao, Y.; Principi, A.; Alonso-González, P.; Carrega, M.; Watanabe, K.; Taniguchi, T.; Vignale, G.; Polini, M.; Hone, J.; Hillenbrand, R.; Koppens, F. H. L. *Nat. Mater.* **2015**, *14*, 421.
(33) Kumar, A.; Low, T.; Fung, K. H.; Avouris, P.; Fang, N. X. *Nano Lett.* **2015**, *15* (5), 3172−3180.
(34) Basov, D. N.; Fogler, M. M.; García de Abajo, F. J. *Science* **2016**, *354* (6309), aag1992.
(35) Chen, J.; Badioli, M.; Alonso-Gonzalez, P.; Thongrattanasiri, S.; Huth, F.; Osmond, J.; Spasenovic, M.; Centeno, A.; Pesquera, A.; Godignon, P.; Zurutuza Elorza, A.; Camara, N.; de Abajo, F. J. G.; Hillenbrand, R.; Koppens, F. H. L. *Nature* **2012**, *487* (7405), 77−81.
(36) Fei, Z.; Rodin, A. S.; Andreev, G. O.; Bao, W.; McLeod, A. S.; Wagner, M.; Zhang, L. M.; Zhao, Z.; Thiemens, M.; Dominguez, G.; Fogler, M. M.; Neto, A. H. C.; Lau, C. N.; Keilmann, F.; Basov, D. N. *Nature* **2012**, *487* (7405), 82−85.
(37) Liu, X.; Bao, W.; Li, Q.; Ropp, C.; Wang, Y.; Zhang, X. *Phys. Rev. Lett.* **2017**, *119* (2), 027403.
(38) Hu, F.; Luan, Y.; Fei, Z.; Palubski, I. Z.; Goldflam, M. D.; Dai, S.; Wu, J. S.; Post, K. W.; Janssen, G. C. A. M.; Fogler, M. M.; Basov, D. N. *Nano Lett.* **2017**, *17* (9), 5423−5428.
(39) Talebi, N.; Ozsoy-Keskinbora, C.; Benia, H. M.; Kern, K.; Koch, C. T.; van Aken, P. A. *ACS Nano* **2016**, *10* (7), 6988−6994.
(40) Nemilentsau, A.; Low, T.; Hanson, G. *Phys. Rev. Lett.* **2016**, *116* (6), 066804.
(41) Zhou, Y.; Chen, R.; Wang, J.; Huang, Y.; Li, M.; Xing, Y.; Duan, J.; Chen, J.; Farrell, J. D.; Xu, H. Q.; Chen, J. *Adv. Mater.* **2018**, *30* (35), 1802551.

DOI: 10.1021/acs.nanolett.8b04242
Nano Lett. 2019, 19, 1009−1014

(42) Xu, X. G.; Ghamsari, B. G.; Jiang, J.-H.; Gilburd, L.; Andreev, G. O.; Zhi, C.; Bando, Y.; Golberg, D.; Berini, P.; Walker, G. C. *Nat. Commun.* **2014**, *5*, 4782.
(43) High, A. A.; Devlin, R. C.; Dibos, A.; Polking, M.; Wild, D. S.; Perczel, J.; de Leon, N. P.; Lukin, M. D.; Park, H. *Nature* **2015**, *522* (7555), 192−196.
(44) Vakil, A.; Engheta, N. *Science* **2011**, *332* (6035), 1291−1294.

DOI: 10.1021/acs.nanolett.8b04242
Nano Lett. 2019, 19, 1009−1014